Korea-Australia Rheology Journal
Vol. 21, No. 4, December 2009 pp. 269-280

Drop formation of Carbopol dispersions displaying yield stress, shear thinning and elastic properties in a flow-focusing microfluidic channel

Joung Sook Hong and Justin Cooper-White
Tissue Engineering and Microfluidics Laboratory, Australian Institute for Bioengineering and Nanotechnology, The University of Queensland, St. Lucia, Qld 4072, Australia

(Received August 3, 2009)

Abstract

The drop formation dynamics of a shear thinning, elastic, yield stress (τ_0) fluid (Carbopol 980 (poly(acrylic acid)) dispersions) in silicone oil has been investigated in a flow-focusing microfluidic channel. The rheological character of each solution investigated varied from Netwonian-like through to highly non-Newtonian and was varied by changing the degree of neutralization along the poly (acrylic acid) backbone. We have observed that the drop size of these non-Newtonian fluids (regardless of the degree of neutralisation) showed bimodal behaviour. At first we observed increases in drop size with increasing viscosity ratio (viscosity ratio = viscosity of dispersed phase (DP) / viscosity of continuous phase (CP)) at low flowrates of the continuous phases, and thereafter, decreasing drop sizes as the flow rate of the CP increases past a critical value. Only at the onset of pinching and during the high extensional deformation during pinch-off of a drop are any differences in the non-Newtonian characteristics of these fluids, that is extents of shear thinning, elasticity and yield stress (τ_0), apparent. Changes in these break-off dynamics resulted in the observed differences in the number and size distribution of secondary drops during pinch-off for both fluid classes, Newtonian-like and non-Newtonian fluids. In the case of the Newtonian-like drops, a secondary drop was generated by the onset of necking and breakup at both ends of the filament, akin to end-pinching behavior. This pinch-off behavior was observed to be unaffected by changes in viscosity ratio, over the range explored. Meanwhile, in the case of the non-Newtonian solutions, discrete differences in behaviour were observed, believed to be attributable to each of the non-Newtonian properties of shear thinning, elasticity and yield stress. The presence of a yield stress (τ_0), when coupled with slow flow rates or low viscosities of the CP, reduced the drop size compared to the Newtonian-like Carbopol dispersions of much lower viscosity. The presence of shear thinning resulted in a rapid necking event post onset, a decrease in primary droplet size and, in some cases, an increase in the rate of drop production. The presence of elasticity during the extensional flow imposed by the necking event allowed for the extended maintenance of the filament, as observed previously for dilute solutions of *linear* polymers during drop break-up.

Key words : yield stress, shear thinning behavior, drop deformation, flow focusing, microfluidics

1. Introduction

Over the last decade, numerous researchers have investigated the potential of microfluidic device technology as a new generation methodology for the continuous and controlled production of droplets. This is principally due to this technology having the proven capability to generate highly monodisperse droplets with precise control over size and production rate, with obvious applications in areas such as micro-scale reactors, mixers, ink-jet printing, drug screening and bio-sensor development. However, in most cases, these applications require the processing of complex fluids, which have nonlinear flow properties that are very different to classical Newtonian fluids. Newtonian fluid models are still, more often than not, used to model and design these devices.

Inherent in the flexibility of microdevice design and construction is the capability to continually (iteratively) modify the device design or configuration to satisfy the desired purpose, regardless of the intrinsic nonlinear flow dynamics of fluids. Due to the analysis of complex flows being reasonably difficult, many researchers have controlled the drop sizes of such complex solutions using external forces, for example electric, ultrasound and magnetic fields, or through variations in the geometric configurations including channel size, *etc* (Li, 2006; Berthier and Silverzan, 2006). Such manipulation unfortunately ignores the utility of the non-Newtonian properties of these fluids to invoke control over droplet size and size distributions. The effects

*Corresponding author: j.cooperwhite@uq.edu.au

of nonlinear flow properties, including shear thinning, elasticity and yield stress, on the dynamics of drop formation and deformation in microfluidic channels requires further investigation in order to understand drop behavior and to generate monodisperse droplets of any fluid, regardless of their non-Newtonian properties.

In this paper we present the experimental results of an investigation into the drop formation of a set of non-Newtonian fluids based on one polymer system, displaying varying degrees of shear thinning, elasticity, and yield stress, in flow focusing microchannels. During the co-flow of two immiscible fluids through a microfluidic channel with an abrupt variation in geometry, a polymeric solution will experience a diverse stress history and as a result, its flow behavior will depart from that displayed by a Newtonian fluid. For example, the resultant decrease in viscosity of a shear thinning solution (with increasing shear or deformation rate), can result in a completely different pinch-off behavior in pendant drop formation (Davidson and Cooper-White, 2006). Thus under the high deformation rate processes associated with the necking of drops from a capillary, the drop formation of a polymeric fluid is expected to be substantially different from a zero shear viscosity matched Newtonian fluid.

Since the early 1900s, research on drop formation and deformation processes under a range of diverse flow conditions has attracted great interest. Initially, most experiments focussed on the deformation and breakup of drops in unrestricted surrounding environments, maintaining a well defined flow field, such as that invoked by a four-roll mill (Taylor, 1932; Han, 1981; Mighri *et al.*, 1997; Levitt *et al.*, 1996; Milliken and Leal, 1991). From such work it has been shown that variations in viscosity ratio, shear thinning and elasticity (characterised by the relaxation time of polymeric solutions) gives rise to very different deformations compared to Newtonian drops and also results in different breakup behaviors. Milliken and Leal (Milliken and Leal, 1991) reported the deformation and breakup of polymeric drops under steady or transient planar flow and compared them with Newtonian drops. Low viscosity polymeric drops do not display the highly deformed, steady drop shapes characteristic of low viscosity Newtonian drops. Under transient deformations, low viscosity ratio polymeric drops formed cusped ends and fragment by tip streaming. Drops of moderate to high viscosity ratio at first stretch like a Newtonian fluid, but thereafter, depending on the magnitude of the Deborah number (=relaxation time × deformation rate), these drops either continue to stretch like a Newtonian drop, forming bulbous ends, or form cusped ends and exhibit a form of tip streaming as they stretch. When tip streaming occurs, the polymeric drop actually fragments in the flow, which is never observed for Newtonian drops in steady flows.

The formation of drops through a capillary nozzle is a well utilized process of forming droplets and particles of high value products in many industrial arenas, for example in ink-jet printing of DNA arrays. Ink-jet technology demands the production of polymeric drops of constant volume and at constant velocity. In this process, the well-known Rayleigh instability results in secondary satellite drops following the primary drop as drops are formed from the capillary nozzle. This process is carried out at high deformation rates, and thus it is expected that Newtonian and non-Newtonian solutions result in completely different drop formation dynamics. However, due to these dynamics being so complex, many theoretical and numerical challenges remain to be solved to explain accurately why many of the observed phenomena occur. Recently, Cooper-White *et al.* performed a study on the drop formation dynamics with well characterized low viscosity polymer (PEO) solutions of varying elasticity, providing detailed insight into the resultant drop formation dynamics, including the length of the filament at the point of detachment and the associated delay time-to-break-up (Cooper-White *et al.*, 2002). Others subsequently have provided detailed investigations into the effects of concentration and molecular weight of aqueous and organic solubilised polymer systems. Basaran and colleagues have simulated computationally the dynamics of drop formation of non-Newtonian liquids, described by separately rate-thinning and rate-thickening functions of Carreau-type equations (Doshi *et al.*, 2003; Suryo *et al.*, 2006; Yildirim *et al.*, 2006). They explained that when rate-thickening dominates, long necks with beads-on-string are developed during detachment of the drop and it also controls the production of satellites of larger number and size. Davidson *et al.* have also numerically investigated the effects of shear thinning on droplet formation, including in particular the resultant neck and filament shape, thickness and length during the evolution of a pendant drop in air (Davidson and Cooper-White, 2006). They described that shear thinning enhances the onset of pinch-off. Liquid flows out of the neck as it thins, due to a curvature-induced pressure increase, by exiting downwards into the drop and upwards into the top of the neck. The continual decrease in the viscosity of the solution with the increasing deformation rate reduces the viscous stresses in the thinning neck, resulting in an increasing dominance of the interfacial stresses over internal viscous stresses, resulting in a more rapid occurrence of pinch-off. However, the role of each of these properties, and that of a yield stress, on the formation and break-up dynamics of droplets of a shear thinning, elastic, yield stress polymer solution, within a microfluidic device remains to be explored.

In this paper we have investigated the drop formation of a dispersion of Carbopol 980 (poly (acrylic acid) (PAA)), displaying shear thinning behavior and a yield stress, in a Newtonian fluid through a flow-focusing microchannel. In order to probe the effect of each of the non-Newtonian traits

of this polymeric solution, the Carbopol solution pH was varied, along with the DP flow rates (from 0.01 through 0.5 ml/hr), whilst both the CP flowrate and viscosity were varied from 0.1 to 4 ml/hr and 0.05~1 Pa.s respectively.

2. Analytical Considerations

In this work, a polymeric drop has been generated within a Newtonian fluid through a flow-focusing microchannel. Flow focusing is one of the most prevalent designs utilised in microfluidic devices to generate a monodisperse droplet distribution, a technique initially introduced by Kamotani *et al.* (Bhunia *et al.*, 1998; Nahra *et al.*, 2000; 2003) and Anna *et al.* (Anna *et al.*, 2003). Nakajima and colleagues (Xu and Nakajima, 2004) further specified the final drop size by introducing the concept of hydrodynamic focusing, narrowing the central stream to a critical width, resulting in controlled breakup of the central stream by Rayleigh instability (Hadamard *et al.*, 1911). In a co-flow condition, such as a flow-focusing geometry, the theoretical description of the drop formation or detachment event is complicated, as many forces are involved. It is necessary therefore to simplify this complex flow condition to analytically predict the drop size and to know which force is dominant in invoking control over the end resulting drop size or drop size distribution.

The role of various forces involved in liquid or gas droplet formation dynamics has been described for Newtonian and some simple model non-Newtonian systems. As the dispersed phase starts to come out through a capillary nozzle, the fluid envelope will continue to expand until the capillary/interfacial forces maintaining attachment (to the nozzle) are balanced with the drag-induced detachment forces. Differences in the velocities and viscosities of both phases determine the magnitude of the drag force driving detachment.

Bhunia *et al.* (Bhunia *et al.*, 1998) analyzed theoretically bubble formation in a co-flowing geometry. They studied the role of various forces involved in the formation of bubbles, including the momentum of the bubble, surface tension, buoyancy, drag, and inertia, according to the following force balance:

$$\frac{d}{dt}\left[\rho_d\frac{\pi}{6}D_d^{\,3}(t)\frac{1}{2}\frac{dD_d(t)}{dt}+\rho_d C_M\frac{\pi}{6}D_d^{\,3}(t)\left(\frac{1}{2}\frac{dD_d(t)}{dt}-U_C\right)\right]+\pi D_{DP}\sigma$$

$$=\rho_d\frac{Q_d^{\,2}}{\frac{\pi}{4}D_{DP}^{\,2}}+\frac{\pi}{6}D_d(t)(\rho_c-\rho_d)g+C_{DW}\frac{1}{2}\rho_c\left(\frac{1}{2}\frac{dD_d(t)}{dt}U_c\right)^2A_{eff} \quad (1)$$

This equation can be reformulated to predict the drop size (D_d) of a polymeric fluid in another fluid, depending on the processing condition and flow geometry, that is the velocities of continuous phase (CP) (U_c) and dispersed phase (DP) ($U_d=dD_d(t)/2dt$), surface tension (σ), viscosities of CP (h_{CP}) and DP (h_{DP}), and diameter of channels (D_{DP}, D_{CP}). If the applied flow condition is a laminar flow and there is no significant density difference between each phase, the buoyancy and inertia forces are not so influential of the result. The drop size can thus be predicted based on the balance of the contributions of the momentum flux ($F_m=\rho_d\frac{Q_d^{\,2}}{\pi D_{HD}^{\,2}/4}$, D_{HD} is the hydrodynamic diameter of DP channel), the surface tension force ($F_\sigma=\Gamma\pi D_{HD}$) and the drag force ($F_D=C_{DW}\frac{1}{2}\rho_c U_{eff}^{\,2}A_H$, $C_{DW}=C_D\frac{1}{(1-D_d^{\,2})^3}$). The drag coefficient, C_D, is assumed to be represented by $24/Re_D$ (as $Re_D<1$ (Berthier and Silverzan, 2006)). Note that $Re_D=r_{cp}U_{eff}D(t)/\eta_{cp}$ and $U_{eff}=U_{CP}-U_D$. If the DP has a different viscosity to the CP, the viscosity ratio (λ, $\lambda=\eta_{DP}/\eta_{CP}$) of DP and CP must also be taken into consideration in order to predict the resultant drop size. The effect of λ is taken into account using a modified drag coefficient ($C_{Deff}=8/Re_D(2\lambda+3)/(\lambda+1)$), introduced by Hadamard (Hadamard *et al.*, 1911) and Rybczinski (Rybczinski, 1911). Based on these assumptions, Eq. (1) is simplified to:

$$\frac{(3+2\lambda)\eta_{CP}}{(1+\lambda)}\left[2v\left(1-\left(\frac{D_{CP}-D_d}{D_{CP}}\right)^2\right)-\frac{1}{2}\frac{dD_d(t)}{dt}\right]$$

$$(\pi D_d)+\rho_{DP}\frac{Q_{DP}^{\,2}}{\pi/4D_{DP}^{\,2}}=\Gamma\pi D_{DP} \quad (2)$$

where D_{CP} is the hydraulic diameter of the continuous phase channel. To further simplify the calculation, the velocity of DP is assumed to be constant. Husny and Cooper-White (Husny and Cooper-White, 2006) defined a factor (ψ), which is an experimental parameter related to the drop growth rate relative to the average CP flow velocity ($\psi=n/U_d$), $0<\psi<2$. It is thus a variable which changes depending on the flow conditions, which will be discussed again in the results section. The contribution of the momentum of the DP is in general small enough to be neglected when the flow rate of DP is low (in our case the maximum flowrate is 0.5 ml/hr). The drop size is thus determined largely by a balance between the drag and interfacial tension forces. The interfacial tension and viscosity ratio (or the viscosity of CP) are thus important parameters for drop size predictions at a fixed flow condition.

The predicted drop size variation with continuous phase flow rate (Q_{CP}) from Eq. (2) as a function of the viscosity ratios and interfacial tension of our experimental system (in the absence of non-Newtonian effects) is shown in Fig. 1(a) and Fig. 1(b), respectively. In Fig. 1(a) the generation of a droplet of viscosity 0.003[Pas] within different viscous CPs, 1[Pas](CP1), 0.1[Pas], and 0.05[Pas](CP2), are compared. These fluid combinations have λ values of 0.003 (=0.003/1.0), 0.03(=0.003/0.1) and 0.06 (=0.003/0.05), respectively. The interfacial tension is fixed to 20.44 [mN/m]. As the viscosity of CP increases, the drop size is dramatically reduced.

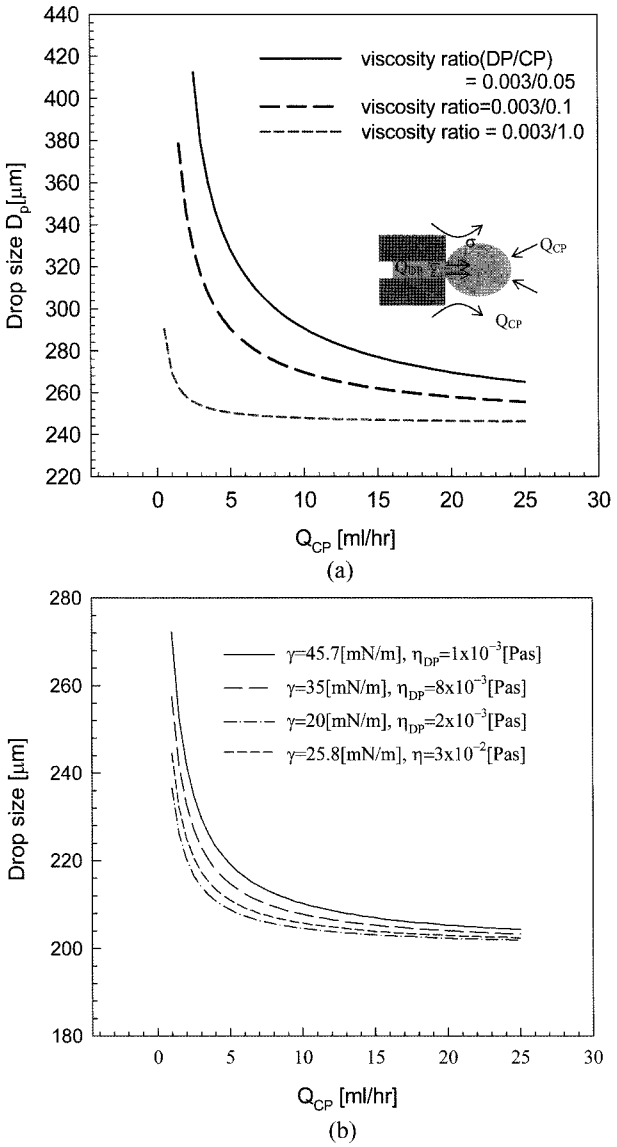

Fig. 1. (a) Effect of viscosity ratio (or η_{CP}) on the drop size and (b) the effect of interfacial tension on the drop size. The drop size is predicted from Eq. (2) depending on the flow rate of CP.

The change in the viscosity of the CP significantly effects the relative contribution of the drag force and hence the resultant drop size. For example, at a CP flow rate of 5[ml/hr], the drop size in CP1 is 250 μm, while in CP2, it is 340 μm. In this calculation, the value of ψ is constant, at a value of 1.7. As the CP flow rate is increased, the resultant drop size is high sensitive to small changes, until the interfacial tension force eventually begins to become comparable to the drag force, with the system gradually approaching the limiting value ($D_{DP} \approx D_{CP}\left(1-\sqrt{1-\frac{\psi}{2}}\right)$) as the flow rate of CP infinitely increases. On the other hand, if the interfacial tension is varied from 45.7 to 20.44[mN/m], again at a CP of 5.0[ml/hr] (at ψ = 1.5), the drop size is only slightly changed (from 215 to 205 μm).

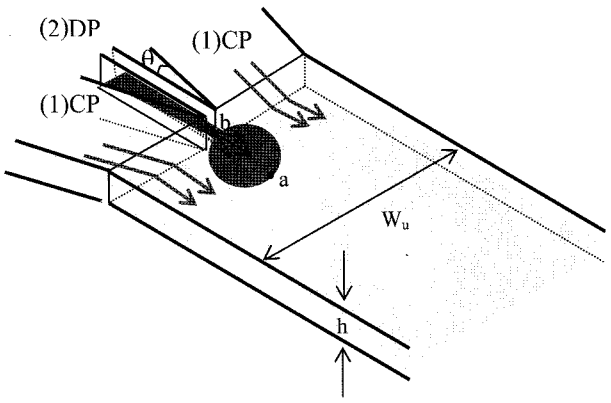

Fig. 2. Schematic diagram of flow-focusing microchannel : W_{DP} =40 μm, Wu=400 μm, h=200 μm, θ=18° and the hydraulic diameter of DP and CP are 67 and 267 μm.

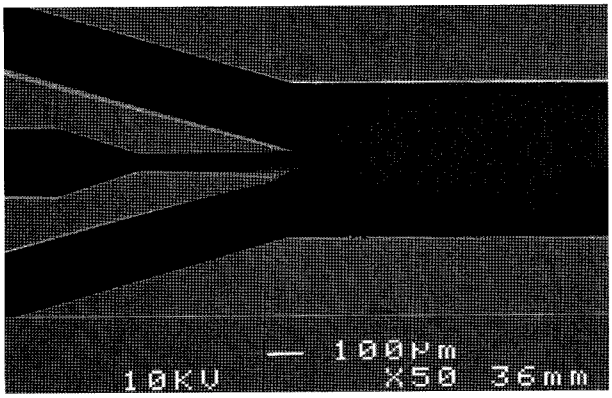

Fig. 3. Top view of flow-focusing microfluidic device. This is taken using a scanning electron microscopy (JSM-6400F, JEOL).

Although simple, this prediction allows us to understand the relative orders of magnitude of each force in their determination of the final drop size. It shows that the drop size is more sensitive to variations in the viscosity of CP rather than interfacial tension. It suggests therefore that the drop size may be able to be further controlled by the introduction of non-linear flow properties of the dispersed phase.

3. Experimental

3.1. Materials

Carbopol (980, Noveon Co.) aqueous dispersions were used as the drop phase (DP) and silicone oil of two different viscosities as the continuous phase (CP). Carbopol is a polymer of acrylic acid $(C_3H_4O_2)_n$ crosslinked with polyalkenyl ethers or divinyl glycol. It presents as microgel particles when solvated in an aqueous solvent. It is known to show a sol-gel transition in aqueous solution as the pH is raised above its pKa (5.5~6.0). Before neutralization, the

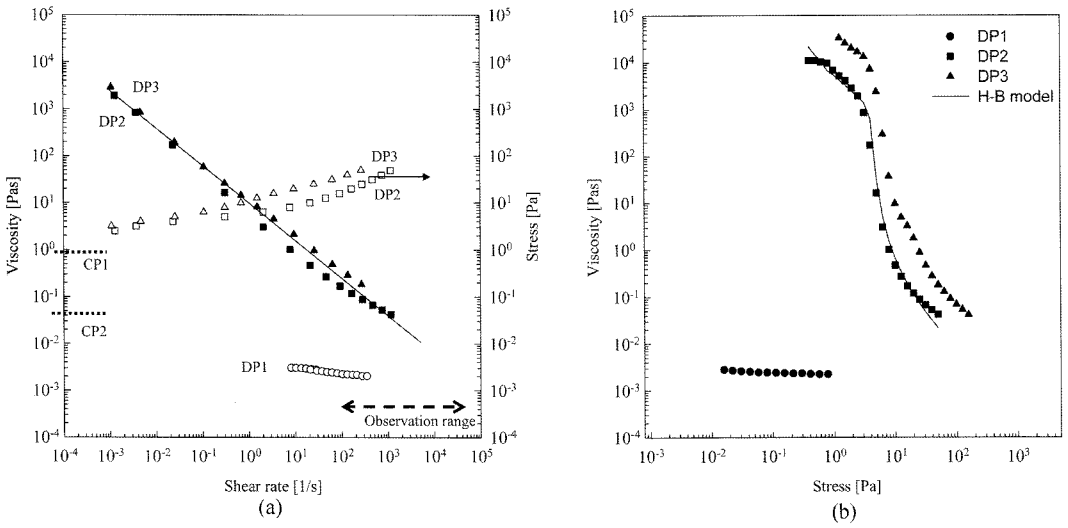

Fig. 4. (a) Steady shear viscosity and stress of Carbopol dispersions. Line represents a fit with Power-law model ($\eta=K\dot{\gamma}^{(n-1)}$). Also includes indications of viscosities of both silicone oil phases and label 'observation range' which shows the shear rate range within the microfluidic device (for the range of flowrates explored). (b) Steady shear viscosity as a function of stress for Carbopol dispersions and prediction with Herschel-Buckley model ($\tau=(K\dot{\gamma}^{(n-1)}+\tau_0(1-\exp(-m\dot{\gamma})))\dot{\gamma}$, here K=5, n=0.2, τ_0=10, and m=100).

Table 1. Materials Properties

Solutions		Description	pH	Viscosity [Pa.s] at 100[1/s]	Yield stress	Relaxation time
Continuous phase	CP 1	1000 cst Oil	-	1	-	-
	CP 2	50 cst Oil	-	0.05	-	-
Dispersed phase	DP 1	0.1 wt% Carbopol solution	3.7	0.00224 [Pas]	-	-
	DP 2	0.1 wt% Carbopol solution	4.7	0.17 [Pas]	2.3 [Pa]	< 1 ms
	DP 3	0.1 wt% Carbopol solution	6.0	0.39 [Pas]	5.7 [Pa]	18.8 ms

Interfacial tension : DP1 Carbopol dispersion (0.1 wt%) in 50 cst oil : 20.44 [mN/m]

dispersions have an approximate pH range of 3.0~3.7 (depending on the polymer concentration) and they display no (measurable) yield stress. The yield stress and viscosity of Carbopol solutions gradually increase with the addition of NaOH and peaks at pH 6.0~6.5. Carbopol solutions were prepared according to Noveon TDS-103 (Noveon, TDS-103) and named as DP1, DP2, or DP3 depending on solution pH (see Table 1).

3.2. Rheological measurements

The rheological properties of the Carbopol dispersions and silicone oils were measured using a TA Instruments G2 rheometer, with both truncated cone-and-plate (40 mm, 2.0°) and a parallel plate (20 mm, gap 1 mm) geometries. A steady stress sweep test and a steady rate test were performed using the parallel plate geometry at room temperature to observe the yield stress and flow behavior of all Carbopol dispersions. The shear viscosity of all Carbopol solutions are shown in Fig. 4. In addition, the extensional behavior of each solution was observed using a CaBER 1 (ThermoHaake, plate of 4 mm diameter, initial gap=2.2 mm, final gap=6.6 mm). The CaBER instrument measures the radius (R_{mid}) in the middle of a cylindrical filament of fluid with time. As a first approximation, the relaxation time (λ) was calculated using the equation below (Rodd *et al.*, 2005; Park, 2003):

$$\frac{R_{min}(t)}{R_1}=\left(\frac{GR_1}{2\sigma}\right)^{1/3}exp[-t'(3\lambda)] \quad (3)$$

where $R_1=R_0(L_f/L_0)^{-3/4}$, σ is surface tension (60 mN/m for DP1 in air), and R_o is the initial radius of the sample. The calculated values are presented in Table 1.

3.3. Interfacial tension

The interfacial tension between the DP1 Carbopol dispersion and silicone oil was measured by a pendant drop method using an OCA20 (DataPhysics). The interfacial tension was assumed constant for all dispersions investigated.

Table 2. Flow Conditions

	Flow rate [ml/hr]	Velocity [m/s]	Shear rate [1/s]	Re_c	Ca	We
Dispersed phase (Q_{DP})	0.01	8.0×10^{-4}	17.3	-	-	-
	0.05	4.0×10^{-3}	86.8			
	0.1	8.0×10^{-3}	173			
	0.5	0.04	868.1			
Continuous phase (Q_{CP})	0.5	2.4×10^{-3}	8.7	3.5×10^{-4}	0.33	1.1×10^{-4}
	1.0	4.8×10^{-3}	17.4	6.9×10^{-4}	0.65	4.5×10^{-4}
	2.0	9.5×10^{-3}	34.7	1.4×10^{-3}	1.3	1.8×10^{-3}
	3.0	0.014	52.1	2.1×10^{-3}	2.0	4.1×10^{-3}
	4.0	0.019	69.4	2.8×10^{-3}	2.6	7.2×10^{-3}

3.4. Fabrication of microchannels

Fig. 2 shows a schematic of the microchannel used in this study. The width of channel 1 (CP channel), channel 2 (DP channel (or nozzle)), and downstream channel (W_u) are 200, 40, and 400 μm respectively, while the channel height (h) is 200 μm. The microdevice was fabricated using standard soft photolithographic procedures using polydimethylsiloxane (PDMS) and an SU-8 photo-resist mold (Li, 2006; Microchem, SU-8 50). The SU-8 mold was fabricated using a high-resolution chrome mask, which resulted in sharp features at channel intersections (as shown in Fig. 3). The PDMS channel was annealed at 65°C to a glass slide that was previously spin-coated with PDMS to seal the device.

A range of flowrates of each phase were investigated. The flowrates for the DP were varied from 0.01~0.5 ml/hr and for the CP, from 0.5~4.0 ml/hr. For each flow rate, the average velocity of the CP in the main channel downstream of the nozzle was calculated based on these channel dimensions. Based on this average velocity, the shear rate ($\dot{\gamma}$), Reynolds number (Re_{cp}), capillary number (Ca) and Weber number (We) were calculated using the following equations (reported in Table 2):

$$\dot{\gamma}=\frac{U_{CP}}{W/2}, Re_{cp}=\frac{\rho_{cp}v_{cp}D_H}{\eta_{cp}}, We=\frac{\rho_{cp}v_{cp}^2D_H}{\sigma}, \text{and}$$

$$Ca=\frac{We}{Re_{cp}}=\frac{v_{cp}\eta_{cp}}{\sigma} \quad (4)$$

The dynamics of drop formation were imaged using a high speed video camera (Phantom V, Vision Research) at a frame rate of 3000 fps, a 60 microsecond exposure time and at a resolution of 1024×256 pixels. The minimum measurable diameter is approximately 8 and 12 μm, *i.e.* 5-7 pixels, using this experimental set-up.

4. Results and Discussion

4.1. Rheological properties of Carbopol dispersions

It is well known that the non-neutralised Carbopol dispersions display near-Newtonian behavior. However, when mixed with sodium hydroxide, the hydroxide ions are recruited into the internal spaces of the Carbopol polymer in order to balance osmotic pressure, resulting in the swelling of the microgel particles, which increases the effective volume fraction occupied by these microgels in solution. This resultant structure produces the observed yield stress (τ_0). The magnitude of the yield stress is thus highly dependent on the degree of neutralization.

The steady shear viscosity of the dispersions investigated in this study as a function of pH, shear rate and shear stress (τ) are shown in Fig. 4(a) and 4(b). We note that DP1 displays, as expected, near-Newtonian behaviour over the range of shear rates and shear stresses explored. Fitting the viscosity curves with a Herschel-Bulkley model ($\tau=K\dot{\gamma}^{(n-1)}+\tau_0(1-\exp(-m\dot{\gamma}))\dot{\gamma}$, *if* $\tau>\tau_0$, K is constant of 10), we note that both DP2 and DP3 have a power law index (n) of approximately 0.2, and that the yield stress of DP2 is 2.3 Pa, whilst it is 5.7 Pa for DP3. For each of these dispersions, when the applied shear stress is higher than the yield stress, the dispersion shear thins. Post yielding, these neutralized solutions (DP2 and DP3) show a high degree shear thinning behavior over the high shear rate region applicable to the rates that will exist in the microdevice (labelled as 'observation range'). Interestingly, whilst the steady shear behavior (post yielding) is similar for these the two fluids, their extensional behaviour, as measured in the CaBER, is quite different (Table 1). DP3 has a relaxation time of 18.8ms. DP2, on the other hand, has a relaxation time of less than 1ms (limit of CaBER measurement).

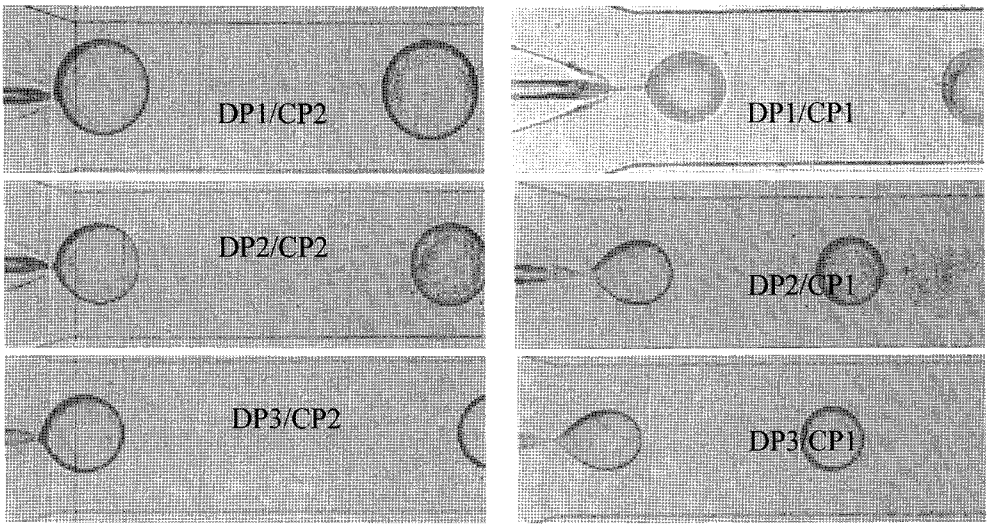

Fig. 5. Drop formation at flow-focusing point at the flow rate ratio (Q_{DP}/Q_{CP}) of 0.05[ml/hr]/0.5[ml/hr]: (a) DPs in CP2, (b) DPs in CP1.

Carbopol dispersions of different rheological character were then used as the dispersed phase to generate drops in the two aforementioned silicone oil phases (CP), using the flow focusing channel shown in Figs. 2 and 3. The CP enters the main channel either side of the DP channel at an angle of 18°. The formation of drops at the capillary tip (or nozzle) depends on the previously described balance of forces. Many dynamics of droplet formation or breaking up will be affected by the viscoelasticity of the DP at particular stages of growth or detachment. Typically, the flow through a microfluidic device is assumed to be laminar ($Re_{CP} << 1$, see Table 2 for velocities, shear rates, Re, Ca and We used in this study). However, as an example, the average shear rate of the DP (based on the average DP velocity) can be as high as 870 s^{-1} in these experiments, which is certainly high enough to elicit differences in the non-Newtonian behaviour of each Carbopol-based dispersed phase during each stage of formation and detachment.

The dynamics of drop formation of these non-Newtonian fluids (Carbopol dispersions) were observed over a wide range of flow rates of each phase. At what will be referred to as low flow rates, the flow rate of CP was fixed at 0.5 ml/hr and the DP flow rate was varied between 0.01 and 0.1 ml/hr. At what will be termed high flow rates, the DP flow rate was fixed at 0.5 ml/hr and the CP was varied between 1.0 and 4.0 ml/hr. Drop formation was performed in two different CPs to observe the influence of the presence of a yield stress in the DP on drop formation and break-up. By comparing these set of fluids, it is possible to investigate the differences in drop growth and pinch-off behavior between such (model) non-Newtonian and Newtonian fluids.

4.2. Drop formation at low flow rates

Fig. 5 presents the pinch-off behavior of drops of DP1, DP2 and DP3 in both CP1 and CP2 at the flow condition of DP=0.05 ml/hr and CP=0.5 ml/hr (DP/CP=0.1). In the case of CP2, all drops (regardless of DP character) are pinched off spontaneously at the capillary tip. There is no filament formation, suggesting that the magnitude of the drag force is too small to competitively induce the formation of a filament post the initiation of necking (it is less than 0.5 Pa). From Fig. 5(a), the drop size of DP2 or DP3 is significantly smaller than for DP1. For a series of Newtonian drops of increasing (zero) shear viscosity, this would indicate an (increasing) difference in interfacial tension, given that all other conditions were similar. However, the interfacial tension of these three systems is not variant. In contrast, the higher viscosity CP1 induces a large enough drag force on the growing drops of each DP stream to couple with the interfacial force to initiate earlier necking (Fig. 5(b)). In the case of DP1, necking is followed by the formation of a thinning capillary filament, that breaks up into several small secondary drops, initiated by a capillary instability. This type of break-up is typically observed during the relaxation of Newtonian fluid column (Xu and Nakajima, 2004). Meanwhile, during detachment of the DP2 or DP3 drops, necking does not extend to the formation of a capillary filament, even though the zero shear viscosities are significantly higher for DP2 and DP3 compared with DP1. A secondary drop is formed in the case of DP2, whilst no secondary drop is formed from the break up of DP3, only a primary drop is formed. The shear thinning nature of each of these two fluids is highly likely to be responsible for the rapid thinning of the neck post onset, and the absence of any capillary filament. The effect of the yield stress, present in both DP2 and DP3 is unclear from these images alone. This comparison does however provide an insight into the effects of shear thinning and elasticity (discussed later) on pinch-off dynamics. In the case of these fluids, these properties are able to influence the

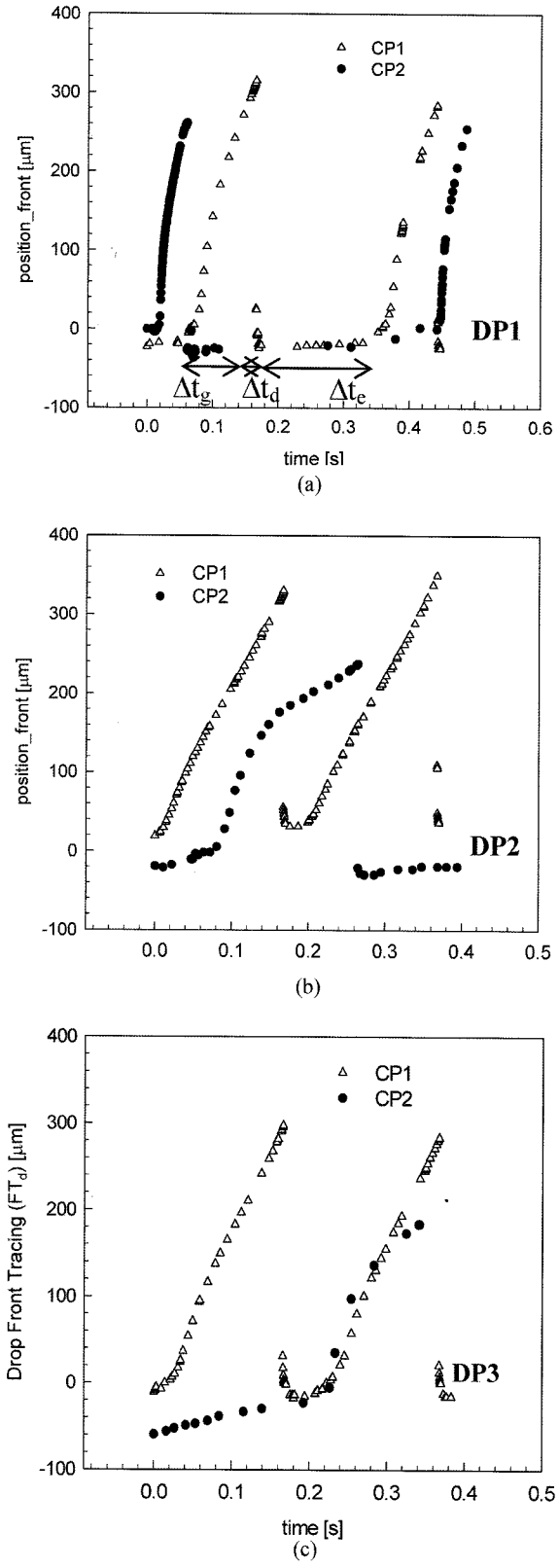

Fig. 6. Front tracing of DP (FT_d) with time in two different continuous phases (CP1, CP2) at fixed flow rate ratio (DP/CP) 0.05/0.5[ml/hr]: (a) DP1, (b) DP2, and (c) DP3. The front of DP is the distance from the flow-focusing point, b in Fig. 2.

pinch-off behaviour of a drop only when the drag force is large enough so as to be able to influence extensional deformation of the neck.

The drop growth rate was thereafter investigated by tracing of the front of the DP stream (point **a** in Fig. 2), at a fixed DP of 0.05[ml/hr] (see Fig. 6). There are three stages of drop formation, with associated timeframes, corresponding to induction (Δt_e), growth (Δt_g), and detachment (incorporating necking and pinch-off) (Δt_d). DP1 has a faster growth rate than either DP2 or DP3, in both CP1 and CP2. However, the interval between drop formation events is much longer. Inspection of Fig. 5 provides some insight into this behaviour, as for fluids DP2 and DP3, the necking does not occur at the nozzle tip, but a small distance along the extended fluid column (that protrudes into the CP). This results in there being less delay between the increase in the fluid volume in the drop, which is initially slow due to the significant capillary force (interfacial tension / capillary radius) just after the pinch-off of a drop.

In the case of DP1 (see Fig. 6(a)), the initial drop growth in both CP1 and CP2 seems similar due to the same interfacial tension, as do the overall shapes associated with this drop growth. There are slight differences in these curves, differences that can only be due to the change of drag force by the increase in viscosity. In particular, the slope of the curve for DP1 in CP1 is substantially steeper than that for DP1 in CP2. In both CP fluids, the DP1 drop grows monotonically with time ($\Delta FT_d/\Delta t \approx$ constant) until the onset of necking is initiated, after which there is a gradual reduction in $\Delta FT_d/\Delta t$ and soon thereafter, pinch off of the drop, at which point the rate of growth returns to zero. The next drop begins to grow as the DP stream continues to flow into the continuous phase. The total timeframe of droplet growth and detachment and the resultant drop generation rate are significantly different in CP1 compared to CP2. Due to the earlier onset of necking of DP1 in CP1, these drops are formed within approximately half of the time as the drops of DP1 and CP2. In particular, the induction time (Δt_e) associated with the initiation of droplet growth is substantially different. This is clear from the data presented in Fig. 6(a).

Meanwhile, for DP2 or DP3, the shape and periodicity of the droplet growth curves are substantially different to DP1, but also differ substantially when the continuous phase is changed from CP1 to CP2 (Fig. 6(b) and 6(c)). The drop growth of DP2 or DP3 in CP2, compared to that in CP1, is much slower and in addition, the growth displays three distinct regions of different slopes, where as in CP1, two regions of different slope, shown as a slight shoulder, are present (as seen in the case of DP1 in both CP1 and CP2).

DP2 and DP3 drops are generated more frequently in CP1 than in CP2, due to the induction time (Dt_e), during which the pressure associated with flow must overcome the Laplace pressure at the nozzle rim, being very short.

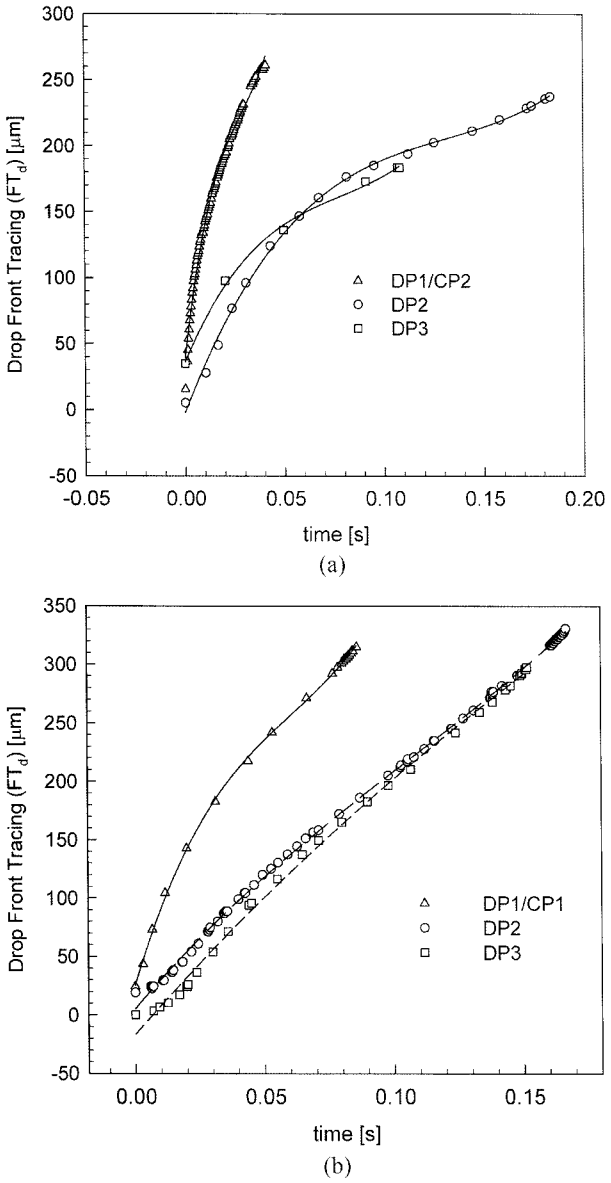

Fig. 7. Comparison of the front tracing of DPs (FT_d) of Fig. 6 in different continuous phases (a) CP2 and (b) CP1.

This is a similar observation as with DP1, the substantive reduction in the induction time with the increase in CP viscosity by a factor of 20. Just after pinch-off, the liquid front of both the DP2 or DP3 streams within CP2 draws back a little towards the nozzle, while the liquid front in CP1 maintains its position without drawing backward.

This recoil suggests that the drag forces imposed on the DP by CP2 are too small to either resist the interfacial tension driving force for recovery of the smallest surface area at the nozzle tip, or below the yield stress of the DP. When a fluid having a yield stress flows through the channel, flow is halted until the shear stress at some position is equal to the yield stress, allowing other forces, interfacial tension for example, to recover shape. Beyond yielding however, the fluid flows through the channel as a shear thinning fluid, as shown in Fig. 4. At the CP flowrate explored, the stress applied by CP2 to the DP stream is around 0.45 Pa, which is much smaller than the stress required to deform either DP2 or DP3 and to induce flow through drag forces on these DP streams, remembering that DP2 and DP3 have yield stresses of 2.3 Pa and 5.7 Pa, respectively.

Fig. 7 compares the drop growth rate data of each DP in CP1 and CP2. The drop growth curves of DP2 and DP3 is particularly sensitive to changes in the CP. From the comparison shown in Fig. 7(a), the growth rate of DP2 and DP3 in CP2 is slower than that of DP1. Although the viscosities of DP2 and DP3 are higher than DP1, it is believed that the presence of a yield stress has a significant effect on these droplet dynamics. Prior to yielding, the shear rate in the bulk of the DP is theoretically zero, although some flow is obviously occurring as the droplet is growing very slowly, likely due to higher wall shear rates allowing fluid flow at the solid-liquid interface (akin to a slip layer). Even though this process in flow controlled, this solid-like flow delays the outflow of a DP into the main downstream channel. Eventually, the drag force being applied by the coflowing continuous phase can overcome the yield stress, at least at the droplet interface (which permeates throughout the bulk eventually), coupling with the pressure provided by the syringe pump associated with the DP, resulting in droplet growth and thereafter breakup. Thus, in CP2, due to the relatively low viscosity of this phase, the impact of the yield stress of the DP results in the drop growth being much slower, as well as effecting pinch-off behavior. On the other hand, when drop formation occurs in CP1, that is twenty times more viscous than CP2, though the drop growth rates are still lower than that observed in the case of DP1, the impact of any yield stress (of DP2 and DP3) is small. The increased drag force by CP1 tends to encourage or stimulate the flow of the DP stream and the growth rate of the droplet is near linear with time (Δt_g in Fig. 6(a)). Thereafter, the slope of the growth rate is changed only slightly during detachment (Δt_d).

Fig. 8 compares the drop size with increasing flow rate of the DPs in two different CPs, CP1 and CP2. The drop size is increased with increases in the flow rate of DP. In CP2, the drop sizes of DP2 and DP3 are smaller than DP1 in all cases, even though their viscosities (and hence viscous pressure within the drop) are much larger than CP2. From the dFT_d/dt_D curves shown in Fig. 6, we note that droplet growth subscribes to the following trend, DP1<DP2<DP3, in terms of the total timeframe associate with droplet formation through to break-off (*e.g.* DP1 = 0.11 s, whilst DP3 = 0.17 s, when in CP2). In CP1, the drop size is overall smaller due to the viscosity ratio being much lower than in the case of CP2. However, the drop sizes of DP2 or DP3 are still smaller than that of DP1, and again we note that droplet growth follows the following trend, DP1 < DP2 < DP3, in terms of the total time-

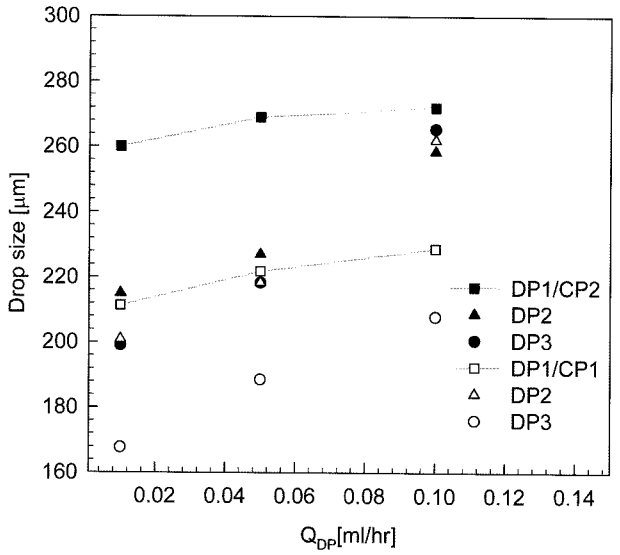

Fig. 8. Comparison of drop size of DPs as a function of the DP flow rate. The flow rate of CP is fixed at 0.5 [ml/hr]. Lines are to guide the eye only.

frame associate with droplet formation through to break-off (*e.g.* DP1= 0.04 s, whilst DP3=0.35 s, when in CP1). The smaller drop sizes are associated with both the presence of a yield stress for each fluid as shown by the large Δt_c's in the case of DP2 and DP3 (increasing from 0.08 s in DP2 to 0.25s in DP3, non-existent in DP1) and the shear thinning nature of these fluids.

From these observations of drop formation under low flow rate conditions, drop formation dynamics are significantly affected by the non-Newtonian properties of the DP, which are overall responsible for the observed differences in drop size.

4.3. Drop formation at higher flow rate region

As the flow rate of DP is increased to 0.5 ml/hr at a fixed CP flow rate of 0.5[ml/hr], the DP stream flows into the CP without break-up. In this case, the drag force associated with the CP is negligible, and in fact, negative due to the differences in velocity between DP and CP. In this case, drag forces do not couple with capillary forces to encourage break-up. The opposite is in fact true. If the flow rate of the CP is increased at this fixed flow rate of DP (0.5 ml/hr), the DP (jet) stream will undergo a reduction in length from the nozzle and produce drops. The flow rate of DP1, DP2, and DP3 were thus fixed at 0.5 ml/hr and that of CP1 varied from 1.0 up to 4.0 ml/hr.

To observe the break-up and generation of secondary drops in detail (at these higher flow rates) during pinch-off, Fig. 9 compares the time evolution of drop formation of DP1, DP2 and DP3 in CP1 from necking to pinch-off at DP=0.5 ml/hr and CP=3.0 ml/hr. When the DP1 drop (our Newtonian-like drop) is pinched off, the necking of the DP stream progresses to form a capillary filament. The thin capillary breaks up first at the proceeding drop interface, and thereafter at the primary drop interface, through the rapid translation of a capillary instability. The instabilities within the now free filament generate several secondary drops by relaxation. Break-up was also noted to be initiated at the primary drop interface in this fluid. In the case of non-Newtonian DP phases, DP2 shows very different pinch-off behavior, dominated by conical thinning of the neck between drops and break-up at the proceeding drop interface, as is typically observed for shear thinning polymeric fluids (Miliken and Leal, 1991). This break-up morphology (akin to tip streaming) generates relatively large secondary drops, resulting in a smaller primary drop

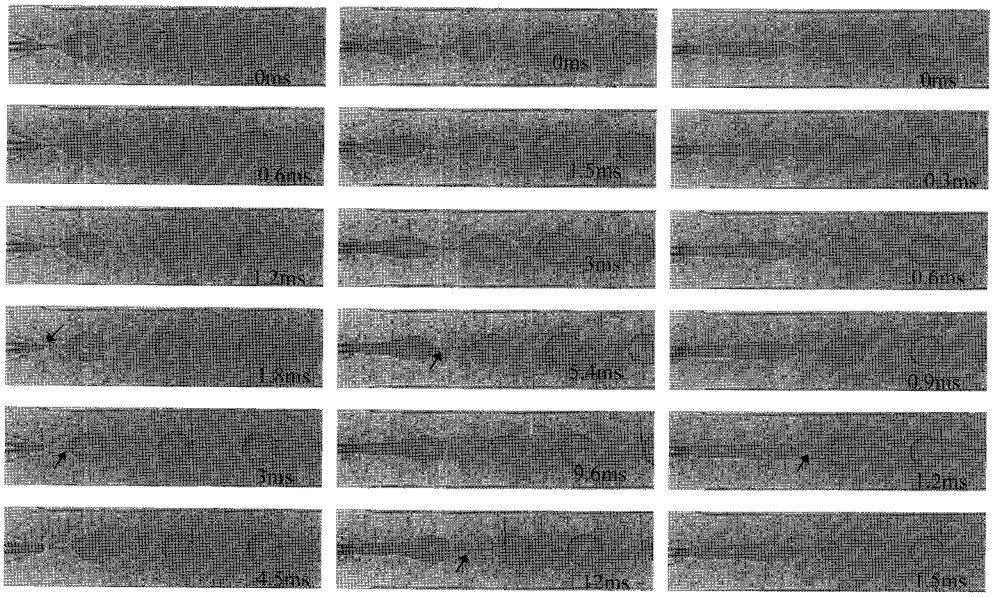

Fig. 9. Time evolution of pinch-off of DP1, DP2, and DP3 in CP1. The arrows indicate the point of break-up of primary or secondary drops.

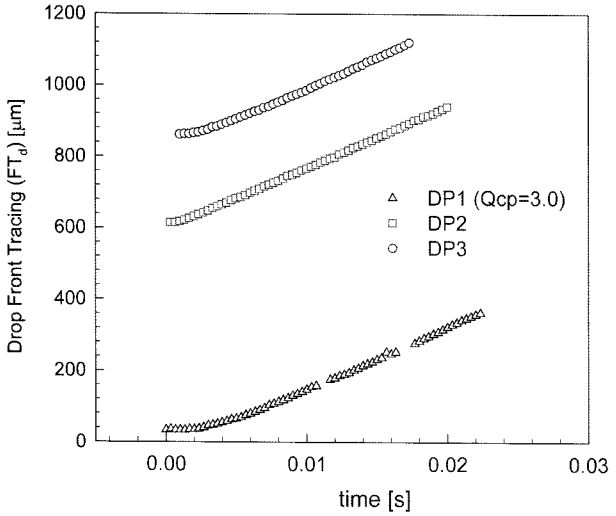

Fig. 10. Front tracing of DPs (FT_d) in CP1 at flow rate ratio, 0.5/3.0[ml/hr]. The front of DP is the distance from the flow-focusing point, b in Fig. 2.

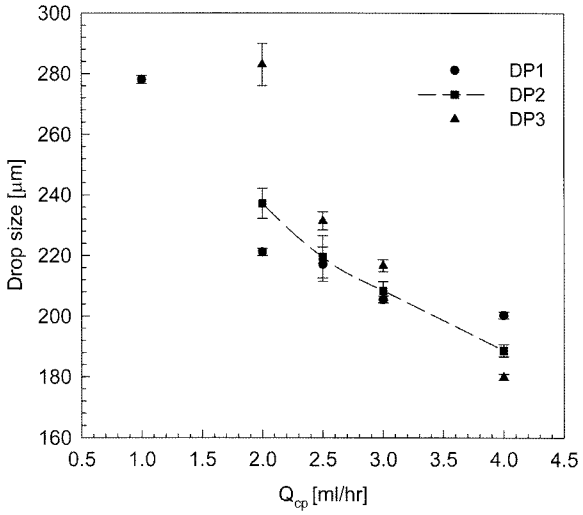

Fig. 11. Variation of drop size of DP1, DP2 and DP3 with the flow rate of CP1. The flow rate of all DPs is fixed at 0.5 [ml/hr]. Lines are to guide the eye only.

compared to a Newtonian DP of equivalent viscosity (at the same shear rate). Note that the time for pinch-off post the onset of necking is also much longer, with most of the pinch-off time being involved in the extension and thinning of the conical filament. Although DP3 displays similar shear behaviour with increasing shear rate as DP2, it shows quite different pinch-off. Post the onset of necking, the thinning of the neck is very rapid, almost as fast as in the case of DP1, until a critical radius after which the neck is substantiated and a cylindrical filament appears, that is extended by the applied drag force from the continuous phase fluid, and thins to below the resolution of our camera without the formation of any secondary drops. This behaviour shows clearly the impact of, firstly, shear thinning at the onset of necking allowing very rapid evacuation of any fluid within the neck region, and thereafter, the impact of fluid elasticity on retardation of pinch off and formation of a cylindrical filament. Similar effects of polymer solution elasticity have been observed in the case of dilute PEO-based low viscosity elastic (Boger) fluids by Cooper-White *et al.* (2002) (Cooper-White *et al.*, 2002) and others subsequently during droplet formation of PEO-aqueous solutions into air from a nozzle.

Besides the difference in pinch-off behavior, the drop growth rate at these higher CP flowrates is also different depending on the non-Newtonian character of each dispersed phase investigated in this study, as shown in Fig. 10. Fig. 10 compares the drop growth rate from the tracing of FT_d at CP=3.0 ml/hr and DP=0.5 ml/hr. The substantial Δt_e or Δt_d observed at lower CP flow rates are no longer present, and the overall time of drop formation is significantly shortened. At these high continuous phase flow rates, even though the position and the morphology of break-up are substantially different, the growth rates (dFT_d/dt_D) of the three DPs are near constant (0.016 for DP1, 0.017 for DP2, and 0.018 for DP3). The local viscosity of the fluid thus determines largely the growth rate of the drop (given that the (equilibrium) interfacial tension does not vary for all of these fluids) and position of break-up in the microchannel.

Over the entire range of continuous phase flow rates (low through to high) explored, the drop sizes DPs are compared as a function of CP1 flowrate (at a fixed DP flowrate of 0.5 ml/hr) in Fig. 12. Comparing fluids of constant Carbopol concentration but varying pH, we note that the DP2 and DP3 drops are larger than those produced from DP1 up to a flow rate of 2.5 ml/hr but are thereafter smaller than DP1 at higher flow rates. Above this critical flow rate, the drop size decreases in line with the increase in viscosity ratio. The drop sizes of DP2 and DP3 are significantly different at low flow rates, with DP3 being 40 microns larger, yet at high flowrates (4 ml/hr), DP3 drops are 15 micron smaller than DP2 drops, assumed to be due to high external drag stresses producing faster reduction in neck thickness (as the fluid shear thins) and the introduction of elastic effects during the detachment of the drop. The elasticity of DP phase thus tends to shorten the drop generation time and prevents the generation of secondary drops. The combination of shear thinning and elasticity within a fluid is responsible for the production of a smaller drop compared to a fluid that presents the same degree of shear thinning or that of a Newtonian equivalent.

5. Conclusions

In this paper, we have observed how the individual non-Newtonian properties of a well known polymeric fluid can be reflected in the drop formation and break-up dynamics when processed as the dispersed phase through a flow-

focusing microchannel. For the range of Carbopol-based fluids investigated in this study, a range of behaviours were observed. As expected, the resultant drop size is substantially affected by changes in the viscosity ratio, increasing with increasing viscosity ratio (viscosity of dispersed phase / viscosity of continuous phase) at low flowrates of the continuous phase. However, as the flow rate of CP increases further, the drop size decreases with increasing viscosity ratio, due to the impact of the non-Newtonian properties of these fluids.

The impacts of the non-Newtonian characteristics of these Carbopol dispersions are best examined through the significant changes in the pinch-off behavior. If the DP is shear thinning, the rate of necking of the DP is significantly enhanced with the extensional deformation imposed by increases in the drag force, coupled with increasing interfacial tension forces (as diameter reduces), which can result in the formation of filaments between drops of conical (as opposed to more cylindrical) morphology. Shear thinning Carbopol fluids produce large secondary drops, when compared to Newtonian-like Carbopol fluids as a result of this thicker filament between the primary and subsequent drop undergoing break-up. Although the size of primary drop is expected to be smaller, as a result of the generation of large secondary drops out of the primary drop, the resulting drop size is not significantly smaller due to the generation time being longer at a constant growth rate.

The presence of a yield stress in a disperse phase fluid (τ_o) only impacts under extremely slow flow conditions of CP (where $\tau_c<\tau_o$), when it effectively slows down the drop growth rate. Post the onset of necking, this slow growth rate couples with the shear thinning properties of these fluids to result in a reduction in final drop size. At higher flowrates, a yield stress does not appear to be influential over drop size or break-up.

The combination of shear thinning and elasticity in a Carbopol dispersion at pH 6.0 allows rapid thinning of the neck post onset, and thereafter maintenance of a cylindrical filament that is further thinned by the imposed drag force. The end result is a smaller primary drop (compared to the dispersion showing only shear thinning) in the absence of any secondary drops, because the drop generation time is shorter.

References

Paul C. H. Li, 2006, *Microfluidic Lab-on a-chip for chemical and biological analysis and discovery*, CRC press.

J. Berthier and P. Silberzan, 2006, *Microfluidics for biotechnology*, Artech House.

M. R. Davidson and J. J. Cooper-White, 2006, Pendant drop formation of shear-thinning and yield stress fluids, *App. Math. Modelling*.

G. I. Taylor, 1932, The Viscosity of a fluid containing small drops of another fluid, Proc Roy Soc London, **A138**, 41.

Han C. D., 1981, *Multiphase Flow in Polymer Processing*, Academic Press, New York.

Mighri F., Ajji A. and Carreau P. J, 1997, Influence of elastic properties on drop deformation in elongational flow, *J. Rheol.*, **41**, 1183-1201.

Levitt. L, Macosko C. W. and Pearson S. D., 1996, Influence of normal stress difference on polymer drop deformation, *Polym. Eng. Sci.*, **36**, 1647-1655.

W. J. Milliken and L. G. Leal, 1991, Deformation and breakup of viscoelastic drops in planar extensional flow, *J. Non-Newtonian Fluid Mech.*, **40**, 355-379.

J. J. Cooper-White, J. E. Fagan, V. Tirtaatmadja, D. R. Lester and D. V. Boger, 2002, Drop formation dynamics of constant low-viscosity elastic fluids, *Non-Newtonian Fluid Mech.*, **106(1)**, 29.

P. Doshi, R. Suryo, O. E. Yildirim, G. H. McKinley and O. A. Basaran, 2003, Scaling in pinch-off of generalized Newtonian fluids, *J. Non-Newtonian Fluid Mech.*, **113**, 1-27.

R. Suryo and O. A. Basaran, 2006, Local dynamics during pinch-off of liquid threads of power law fluids: scaling analysis and self-similarity, J. Non-Newtonian Fluid Mech., **138**, 134-160.

O. E. Yildirim, O. A. Basaran, 2006, Dynamics of formation and dripping of drops of deformation-rate-thinning and –thickening liquids from capillary tubes, *J. Non-Newtonian Fluid Mech.*, 136, 17-37.

A. Bhunia, S. Pais, Y. Kamotani and I. Kim, 1998, Bubble formation in a coflow configuration in normal and reduced gravity, *AIChe J.* **44**, 1499-1509.

H. K. Nahra and Y. Kamotani, 2000, Bubble formation from wall orifice in liquid cross-flow under low gravity, *Chem. Eng. Sci.* **55**, 4653-4665.

H. K. Nahra and Y. Kamotani, 2003, Prediction of bubble diameter at detachment from wall orifice in liquid cross-flow under reduced and normal gravity conditions, *Chem. Eng. Sci.*, **58**, 55.

S. L. Anna, N. Bontoux and H. A. Stone, 2003, Formation of dispersions using "flow focusing" in microchannels, *App. Phy. Lett.*, **82(3)**, 364-366.

Q. Xu, M. Nakajima, 2004, The generation of highly monodisperse droplets through the breakup of hydrodynamically focused microthread in a microfluidic device, *App. Phy. Lett.*, **85(17)**, 3726-3728.

L. Rayleigh, On the capillary phenomena of jets, *Proc. R. Soc.*, **29**, 71-97.

J. Hadamard, 1911, Measurement permanent lent d'une sphere liquide et visqueuse dans un liquide visquex, *CR Acad. Sci.*, 1735.

W. Rybczynski, 1911, Translatory motion of a fluid sphere in viscous medium, *Bull. Int. Acad. Pol. Sci. Leu. CI Sci. Nat. Ser.* A 40.

J. Husny and J. J. Cooper-White, 2006, The effect of elasticity on drop creation in T-shaped microchannels, J Non-Newtonian Fluid Mech..

Noveon, TDS-103, http://www.personalcare.noveon.com/techdata/Carbopol980.asp.

L. E. Rodd, T.P. Scott, J. J. Cooper-White and G.H. McKinley, 2005, Capillary break-up rheometry of low-viscosity elastic fluids, Appl. Rheol., **15**, 12-27.

A. E. Park, 2003,Capillary breakup of food stuffs and other complex fluids, MS Thesis, MIT, Cambridge(USA).

Microchem, SU-8-50, http://www.microchem.com/products/su_eight.htm.